

Article

Track False-Target Deception Method Based on Phase-Switched Screen

Guoqing Hao, Dejun Feng *, Junjie Wang, Zimeng Zhou and Ling Wang

The State Key Laboratory of Complex Electromagnetic Environment Effects on Electronics and Information System, National University of Defense Technology, Changsha 410073, China; haoguoqing21@nudt.edu.cn (G.H.)
* Correspondence: fdj117@nudt.edu.cn; Tel.: +86-13974863862

Abstract: Track processing is the foundation of radar multi-target tracking, and the processing performance for jamming has particular research significance when it comes to protecting high-value targets. At present, passive jamming using a modulated metasurface exhibits a fast response and a flexible operation mode. However, most research in this area has been carried out at the radar signal processing level and less at the data processing level. In this paper, a range of false target track deception method based on a phase-switched screen (PSS) is proposed, and the relationship between the matched filtering output, radar detection, and track processing is derived. This method uses PSS to generate multiple false targets with controlled spatial distribution and magnitude, which can form high-fidelity false tracking tracks. The number of false tracking tracks can be flexibly altered by controlling the modulation parameters. The simulation results validate the effectiveness of the proposed method.

Keywords: phase-switched screen (PSS); false tracking tracks; multiple false targets; modulation parameter

1. Introduction

As the basis of radar multi-target tracking, track processing enables the tracking and prediction of a target's track [1]. To improve the survival rate of high-value targets, researchers have conducted numerous studies on radar track deception techniques. The current technology can simultaneously achieve three dimensions of range, speed and angle deception, offering a high degree of realism for the false track. Thus, it can disrupt the opponent's radar search and tracking [2–4]. Accordingly, it has become one of the current research hotspots in the field of radar jamming.

At present, track spoofing technology is mainly implemented through active forwarding devices. It uses digital frequency memory (DRFM) to sample and store the received signal, followed by delayed forwarding according to certain rules. It eventually displays a false track on the opponent's radar display [5–7], tricking the radar into searching and tracking and wasting its limited resources. However, active devices are costly to design and require the interception of priori information, making practical work more complex.

Instead of actively radiating the electromagnetic waves signal [8,9], passive jamming devices can alter the scattering pattern of the electromagnetic waves using devices such as angle reflectors and chaff. Conventional passive devices have a single fixed electromagnetic characteristic after processing, making them unable to meet the requirements of real-time with flexible regulation.

With the continuous development of electromagnetic modulation technology, metamaterials with peculiar physical properties have emerged. The frequency selective surface [10–12], phase-switched screen [13–16], coding metasurface [17–19], and many other types of metasurfaces can achieve multi-dimensional and different degrees of modulation in radar-received electromagnetic waves. As a new electromagnetic material, the



Citation: Hao, G.; Feng, D.; Wang, J.; Zhou, Z.; Wang, L. Track False-Target Deception Method Based on Phase-Switched Screen. *Electronics* **2023**, *12*, 2996. <https://doi.org/10.3390/electronics12132996>

Academic Editor: Yide Wang

Received: 12 May 2023

Revised: 4 July 2023

Accepted: 5 July 2023

Published: 7 July 2023



Copyright: © 2023 by the authors. Licensee MDPI, Basel, Switzerland. This article is an open access article distributed under the terms and conditions of the Creative Commons Attribution (CC BY) license (<https://creativecommons.org/licenses/by/4.0/>).

phase-switched screen (PSS) has unique physical properties (e.g., a negative refractive index, negative permittivity) [20]. By modulating the material in the X-band and Ku-band, the radar echo can be altered to affect the radar's measurement of the true state of the target [21]. Through theory and simulation, researchers have demonstrated that PSS has excellent wave absorption properties in the X-band frequency and can reduce radar targets' radar cross section (RCS) to achieve electromagnetic invisibility. [22]. By controlling the signal to periodically change both the absorption and reflection states of the PSS, Feng et al. created a multi-false target generation method that achieved deceptive jamming in the velocity, angle, and other dimensions [23–26]. Fan et al. achieved the consumption of radar resources by modulating the metasurface during the radar search phase [27]. The above research shows that PSS can generate multiple false targets and has promising applications in the field of radar jamming.

Inspired by the above ideas, the objective of our study was to propose a track deception jamming method for a range of false targets based on PSS. This method used PSS to generate multiple false targets with controlled spatial distribution and amplitude to induce the opponent radar to detect and track these targets. This resulted in stable false tracking tracks, which increased the workload of radar track processing and consumed radar system resources. The novelty of this work was that the number of false tracks could be flexibly controlled by varying the modulation parameters of the PSS. Compared to active jamming, this method did not require the prior acquisition of priori information and, thus, was less complex.

2. PSS Electromagnetic Regulation

PSS is a new type of wave-absorbing material, mainly consisting of a switching impedance layer, a media layer, and a metal conductor backing plate, whose structure is shown in Figure 1. The switching impedance layer generally consists of an active impedance layer that can switch between fully transmitted and fully reflected states. When these two states are switched intermittently, it is possible to change the signal energy to zero at the original incident wave carrier frequency. Additionally, controlled harmonic components are generated in its vicinity, which can be considered false targets by the radar receiver. By controlling the frequency of the PSS switch, the distribution of these harmonic components can be changed. At this point, it was assumed that the energy in the band of the real target shifted to other frequency bands, creating false targets to achieve a deceptive jamming effect.

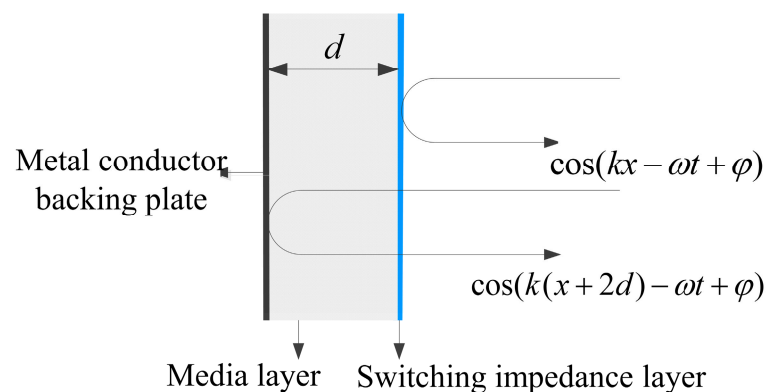


Figure 1. PSS structure diagram.

We assumed that the electromagnetic wave was vertically incident and that its carrier frequency was ω and wavelength was λ , and the wave vector was $k = \omega/c = 2\pi/\lambda$. The dielectric constant of the PSS dielectric layer was one, and its thickness was $d = \lambda/4$. When the switching impedance layer acted as a total reflection state, the reflected electromagnetic wave could be expressed as $\cos(kx - \omega t + \varphi)$. When it behaved in a fully transmissive state,

the electromagnetic wave could completely pass through the switching impedance layer. The reflected electromagnetic wave was then reflected by the metal base plate, at which point the reflected electromagnetic wave could be expressed as $\cos(k(x + 2d) - \omega t + \varphi) = \cos(kx - \omega t + \varphi + \pi)$. In this case, the phase difference of the reflected electromagnetic wave in these two states was exactly π . Notably, however, when x and the initial phase φ were 0, the phases of the two echoes were opposite. Thus, the PSS could be equated to a phase-modulated signal in the form of a bipolar rectangular pulse and applied by the PSS to the incident electromagnetic wave during periodic switching. The modulated signal model is shown in Figure 2. The amplitude values in the graph were +1 and -1, corresponding to the PSS's fully reflective and fully transmissive states, respectively.

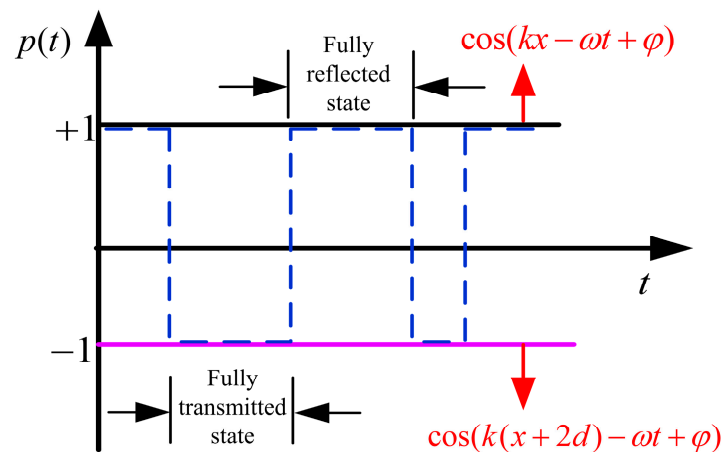


Figure 2. PSS modulation signal model.

Assuming that the PSS was under the control of a modulation function of two states' uninterrupted switching, the reflected signal was subject to phase modulation. Simply, the modulated signal was set as a periodic rectangular square wave, whose time domain expression could be expressed as:

$$p(t) = A_0 + \sum_{n=1}^{+\infty} A_n \sin(2\pi n f_s t) \tag{1}$$

where $A_0 = |2\tau/T - 1|$, $A_n = 2/n\pi(1 - \cos(2n\pi\tau/T))$; T is the modulating signal period, $f_s = 1/T$ represents the modulating frequency, and τ/T represents the duty ratio of the modulating signal. The frequency domain expression of the signal was:

$$P(f) = A_0\delta(f) + \sum_{\substack{n=-\infty \\ n \neq 0}}^{+\infty} A_n\delta(f - n f_s) \tag{2}$$

When an electromagnetic wave is vertically incident on a PSS, the time domain of the return signal can be expressed as

$$r(t) = s(t) \times p(t) \tag{3}$$

The frequency domain expression for the echo signal was:

$$R(f) = S(f) \otimes P(f) = A_0S(f) + \sum_{\substack{n=-\infty \\ n \neq 0}}^{+\infty} A_nS(f - n f_s) \tag{4}$$

According to Equation (4), the PSS-modulated echo signal produced several harmonic components symmetrical with the center frequency $\sum S(f - nf_s)$. They could be seen as multiple false targets.

This assumed that the incident signal was the linear frequency modulation (LFM) signal, the pulse width was T_p , and the modulation frequency was K_r . Its carrier frequency and signal bandwidth were defined as f_0 and B , respectively. The time domain expression was:

$$s(t) = \text{rect}\left(\frac{t}{T_p}\right) \exp\left[j2\pi\left(f_0t + \frac{1}{2}K_r t^2\right)\right] \tag{5}$$

where $\text{rect}(\cdot)$ indicates a rectangular pulse.

The radar receiver underwent matching filtering to maximize the output signal-to-noise ratio (SNR) after obtaining the echo signal. Matched filtering is essentially a band-pass filter, the bandwidth of which is generally set in the frequency range of the reflected signal. Its range can be expressed as $[f_0 - B/2, f_0 + B/2]$. Additionally, PSS is capable of a frequency shift, and thus, the sideband nearest to the carrier frequency was set at $f_0 \pm f_s$. Therefore, the frequency ranges of these two sidebands were $[f_0 - B/2 + f_s, f_0 + B/2 + f_s]$ and $[f_0 - B/2 - f_s, f_0 + B/2 - f_s]$, respectively. When $f_s > B$, the generated sidebands were outside the filter’s passband. At this point, the radar could not detect the existence of the target; therefore, it was not possible to achieve false target jamming. When $f_s < B$, the radar receiver received the upper and lower sidebands of the echo signal. Additionally, the smaller the modulated signal frequency, the more the sideband components entered the radar receiver. Therefore, in this paper, the modulation frequency was set to $f_s < B$ so that the reflected signal spectrum was within the passband of the radar receiver.

According to the analysis in Ref. [16], although the frequency of the LFM signal varied with time, it was basically guaranteed that the phase difference between the front and rear beams was approximately π . Therefore, the overall modulation performance was not affected.

The reflected signal became the baseband signal after mixing and filtering in the radar receiver. The echo baseband signal was:

$$r(t) = \text{rect}\left(\frac{t}{T_p}\right) \exp(j\pi K_r t^2) \times \left[A_0 + \sum_{\substack{n=-N \\ n \neq 0}}^{+N} A_n \exp(j2\pi n f_s t) \right] \tag{6}$$

where $N = \lfloor B/f_s \rfloor$, $\lfloor \cdot \rfloor$ means rounded by 0, and the baseband signal can be seen as the sum of multiple LFM signals by the Doppler shift. The final result of the matched filtering could be expressed as

$$I_{r(t)} = A_0 \left(1 - \left|\frac{t}{T_p}\right|\right) \text{sinc}\left[K_r T_p \left(1 - \left|\frac{t}{T_p}\right|\right)\right] + \sum_{\substack{n=-N \\ n \neq 0}}^{+N} A_n \left(1 - \left|\frac{t}{T_p}\right|\right) \text{sinc}\left[K_r T_p \left(1 - \left|\frac{t}{T_p}\right|\right)\right] \left(t + \frac{n f_s}{K_r}\right) \tag{7}$$

As demonstrated by Equation (7), the matched filtered output contained many sinc discrete peaks where n represents the order of these discrete peaks. The interval between the peaks of each order was:

$$\Delta t = \frac{f_s}{K_r} \tag{8}$$

The magnitude of each order of peak was:

$$|y_n(t_{\max})| = \frac{1}{n\pi} \left(1 - \cos\left(\frac{2n\pi\tau}{T}\right)\right) \left(1 - \frac{|n f_s|}{B}\right) \tag{9}$$

As shown by Equations (8) and (9), the range between the peaks could be determined by the modulation frequency f_s ; due to hardware conditions, $n f_s$ was generally much smaller than the signal bandwidth B , and the peak amplitude was mainly determined by

the duty ratio τ/T . The prototypes of Equations (1)–(9) in this paper were sourced from Ref. [26].

3. Methods and Assessment Indicators

The echo signal was matched and filtered, and then CFAR detection was performed for target detection. It generated adaptive thresholds that could be adjusted for background noise, clutter, and interference by estimating the average level of the reference unit. The most commonly used CFAR algorithm is cell average (CA), and its detection performance is usually expressed in terms of detection probability. The spatial distribution and amplitude of the false targets generated by PSS are relatively stable when the modulation frequency and duty ratio are determined. Therefore, it was not a random variable, and its probability density function cannot be obtained. Accordingly, this paper used the detection threshold to determine the detection performance of CFAR.

The sampling functions of the matched filter can be described as

$$F_s(t) = I_{r(t)} \times \sum_{n=t_1}^{n=t_2} \delta(t - nT_s) \tag{10}$$

When the radar detected a target signal, the protection unit was an area used to avoid noise interference. This is usually defined as a window, and the target signal is detected in the center of the window. The role of the reference unit was to calculate statistical information about the background noise.

Assuming that the number of reference units in CA-CFAR detection was $2k_t$, the number of protection units was $2k$, the threshold factor was η , and the detection threshold T_h could be expressed as:

$$T_h(n) = \eta \times \frac{\sum_{i=n-k-1}^{i=n-k-kt} F_s(i) + \sum_{i=n+k+1}^{i=n+k+kt} F_s(i)}{2k_t} \tag{11}$$

The the moment n_1 had

$$F_s(n_1) \geq T_h(n_1) \tag{12}$$

This indicated that the false target had passed CFAR detection.

The track processing of the target began after target detection. The key to track processing was the selection of the tracking wave gate T_c . The range between false targets passed through the tracking wave gate under the following conditions:

$$V\Delta t = \frac{f_s}{K_r} V > T_c \tag{13}$$

where V is the speed of movement.

As demonstrated, when Equations (12) and (13) were satisfied simultaneously, the false target could be detected by the radar and form a false tracking track.

In multi-target tracking, the track management function of data processing plays a very important role. It can terminate some tracks according to certain rules, exit tracking, and prevent the radar from collapsing due to a large amount of interference and bait from the enemy. It is also possible to perform precise tracking on certain key targets, ensuring timely and accurate strikes against threatening targets.

Data processing creates a track for each target. This is equivalent to creating a file for each target, which can store a lot of information about the target. By utilizing the information of the target trajectory and the current detection and measurement processing results, data processing could, on the one hand, continuously and stably track the target; on the other hand, it could achieve pairing and an association between the current detection point and existing tracks. Track management is a key step when processing radar data, including track initiation, track association, and track tracking. In the case of multiple

false target jamming, both free tracks and unconfirmed sets of tracks with a failed track association could start a temporary track. Although these temporary tracks only remained in the computer for a short time, they increased the burden of radar data processing and consumed radar system resources.

The temporary tracks generated during radar track initiation and the tracking tracks generated during tracking reflected the current workload of radar data processing. They could be used as indicators for assessing the deceptive jamming of multiple false target tracks. Assuming that M Monte Carlo experiments were conducted, the average number of temporary tracks for the M experiments could be expressed as

$$L_{tr} = \frac{\sum_{i=1}^M T_i}{M} \quad (14)$$

where T_i is the number of temporary tracks formed in the i -th simulation.

The average number of tracking tracks for M experiments could be expressed as

$$L_{te} = \frac{\sum_{i=1}^M T_{ei}}{M} \quad (15)$$

where T_{ei} is the number of tracking tracks formed in the i -th simulation.

4. Results

4.1. Simulation Parameter Setting

This section uses a simulation analysis to validate the proposed PSS modulation method for jamming radar tracks. The simulation parameters of LFM and CFAR are shown in Table 1. The number of real targets in the simulation space was two. The RCS of the targets was generated randomly and did not vary with time. The targets always maintained a uniform linear motion.

Table 1. Simulation parameters.

Parameter	Value (Unit)	Parameter	Value (Unit)
Carrier frequency (f_0)	6 (GHz)	Pulse duration (T_p)	50 (us)
Signal bandwidth (B)	10 (MHz)	Reference units	64
Chirp rate (K_r)	2×10^{11} (Hz/s)	Protection units	8

A radar display for multiple target tracking is shown in Figure 3. The blue curves in Figure 3 indicate the tracks generated by the radar tracking target. The modulation duty ratio and modulation frequency of PSS were defined as 0.5 and 20 KHz, respectively. As shown in Figure 3, the PSS-modulated targets produced multiple parallel false tracks in motion. Each track produced by this method is clearly presented in the radar display.

4.2. The Effect of Modulation Signal Frequency on the Deception Effect

As demonstrated by the basic principles of PSS electromagnetic modulation in Section 2, the key parameters included the modulation frequency and duty ratio. Next, we present a primary analysis of the modulation frequency's effects. The PSS alters the radar return by actively modulating the electromagnetic waves, creating false targets, and impacting radar track management. The simulation of radar tracking targets was conducted using MATLAB software. The number of Monte Carlo simulations was 500, the duration of the target motion was 20 s, and the modulation duty ratio was 0.5. The output envelope demodulation and CFAR detection gates at modulation frequencies of 10 KHz and 20 KHz, respectively, are shown in Figure 4.

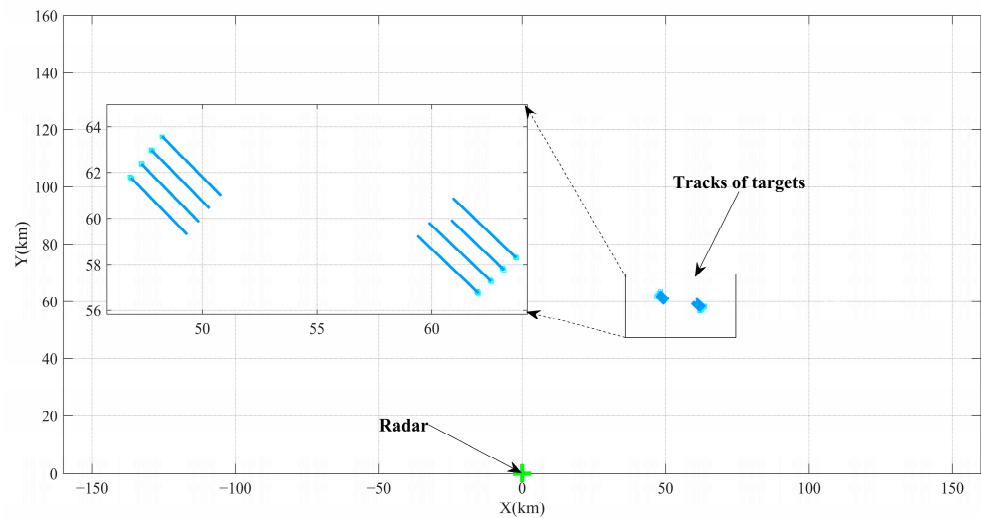


Figure 3. The radar display for multiple target tracking.

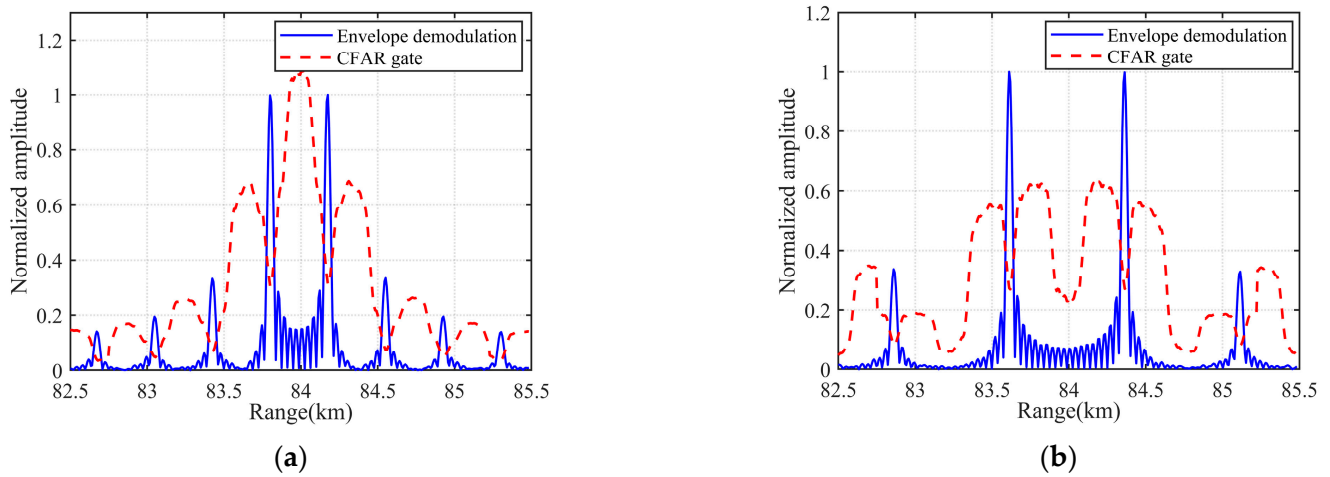


Figure 4. The number of false targets that passed at different modulation frequencies. (a) $f_s = 10$ KHz, $\tau/T = 0.5$; (b) $f_s = 20$ KHz, $\tau/T = 0.5$.

Based on Figure 4, it can be concluded that the real target vanished as a result of the modulation effect of PSS. The modulated radar envelope demodulation resulted in multiple peaks that were symmetrically distributed about the real target. These output peaks could be considered multiple false targets generated by the PSS modulation. The spatial distribution of the false targets changed with the modulation frequency. In simple terms, the distance between the false targets increased with the modulation frequency.

As seen in Section 3, the false targets were track processed after passing CFAR detection. To further analyze the effect of the modulation frequency on the deception effect, the simulation set the duty ratio constant and changed the modulation frequency of the PSS modulation signal. The number of radar false tracking tracks, true tracking tracks, and temporary tracks for different modulation frequencies is shown in Figure 5.

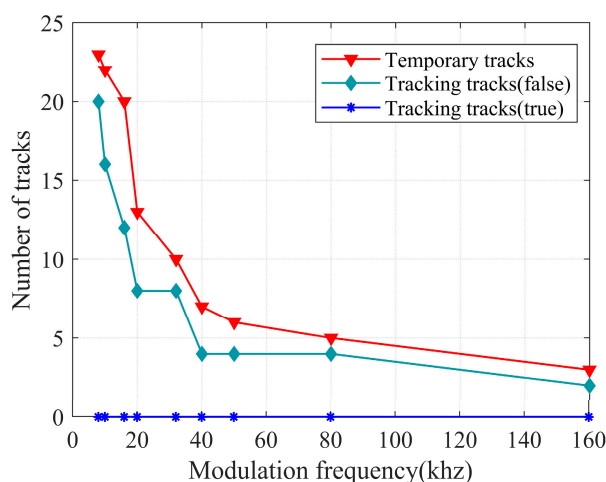


Figure 5. The effect of modulation frequency on radar tracks.

The following conclusions can be drawn from Figure 5. When the duty ratio was 0.5, the real target faded; therefore, the resultant tracking tracks were all false tracks. As the modulation frequency increased, the number of false and temporary radar tracks gradually decreased. Additionally, the variation in the number of both tracks was greater at lower modulation frequencies. As demonstrated by the principle of PSS modulation, the spatial distribution of the false target could be related to the modulation frequency. The range between the false targets was closer when the modulation frequency was lower. More false targets could be received within the radar reception's bandwidth, generating more false and temporary tracks. When the modulation frequency gradually increased, the range between the false targets became sparse, and the number of false targets received by the radar decreased. In addition, the number of false tracks did not change significantly when the modulation frequency increased to a certain value. This was because only the main false target fell within the radar reception bandwidth.

4.3. The Effect of Modulation Signal Duty Ratio on the Deception Effect

The duty ratio of the modulated signal is another important parameter of the PSS, which affects the amplitude of each order of the false target. Generally, the lower the duty ratio, the smaller the difference in magnitude between the higher-order and lower-order false targets, which can appear as a group of false targets with comparable energy; when the duty ratio is high, the higher-order pseudo targets can behave like several lower-order pseudo targets with higher energy. Figure 6 shows the output envelope demodulation and CFAR detection gates for the modulation frequencies of 10 KHz and duty ratios of 0.1 and 0.35.

As seen in Figure 6, a change in the duty ratio influenced the magnitude of each order of the false target. However, the number of multiple false targets generated through PSS modulation remained the same in both cases, and the spatial distribution did not change, which also verified the previous analysis. By comparing the two subplots, it could be found that the change in the magnitude of the false targets of each order caused fluctuations in the detection threshold, resulting in more false targets passing detection. Figure 6b exhibits five more false targets which passed detection compared to Figure 6a, which showed a better modulation effect.

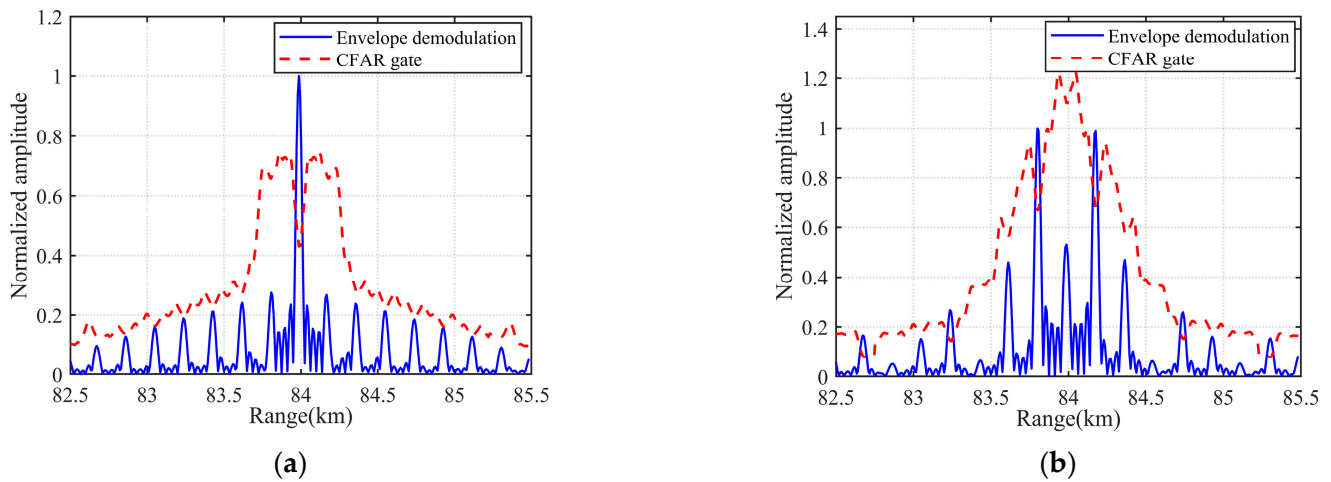


Figure 6. The number of false targets passed at different duty ratios. (a) $f_s = 10$ KHz, $\tau/T = 0.1$; (b) $f_s = 10$ KHz, $\tau/T = 0.35$.

The effect of the modulated signal duty ratio on track deception is analyzed below. Figure 7 presents the relationship curves between the duty ratio and the number of radar false tracking tracks, real tracking tracks, and temporary tracks when the modulation frequency was 10 KHz.

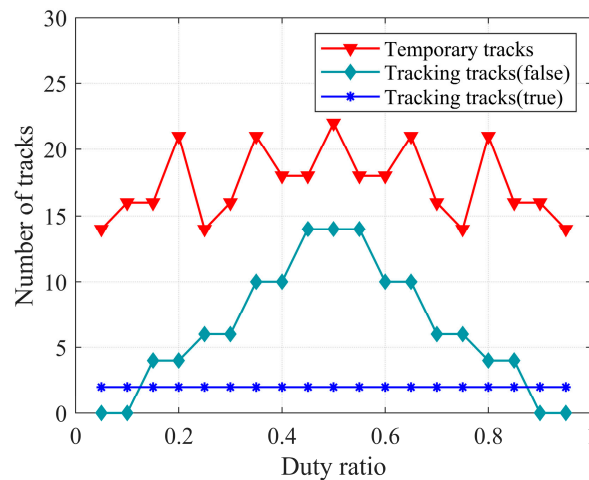


Figure 7. The effect of modulating the duty ratio on radar tracks.

The following conclusions can be drawn from Figure 7. First, the number of false and temporary tracks was symmetrically distributed, with 0.5 as the center. Utilizing the PSS modulation principle, at duty ratios of 0.2 and 0.8, the same modulation effect occurred, resulting in the same number of two tracks being produced. Second, for a duty ratio of 0~0.5, the number of false tracks increased with the increase in the duty ratio. The difference in the number of false and temporary tracks was significant when the duty ratio was small. This was because many false targets failed to pass radar detection but still had an effect on the radar track’s initiation, generating many temporary tracks. For example, at a duty ratio of 0.2, there were only four false tracking tracks, but the number of temporary tracks could reach twenty-one. Third, the duty ratio affected the false tracks at this modulation frequency more significantly. The duty ratio could affect the number of false targets detected through the radar, which was directly related to the number of false tracking tracks.

4.4. Analysis of Deception Effect with Different Number of Targets

The performance of radar track processing is usually related to many factors, such as the density of targets, the number of targets, etc. To further analyze the deception effect under different scenarios, the simulation set the modulation frequency to 80 KHz and the duty ratio to 0.3. PSS's modulation effect generated two false targets on both sides of the real target. Figure 8 showcases the relationship between the tracked tracks (with and without interference cases) and the temporary tracks with the number of real targets in the case of PSS modulation.

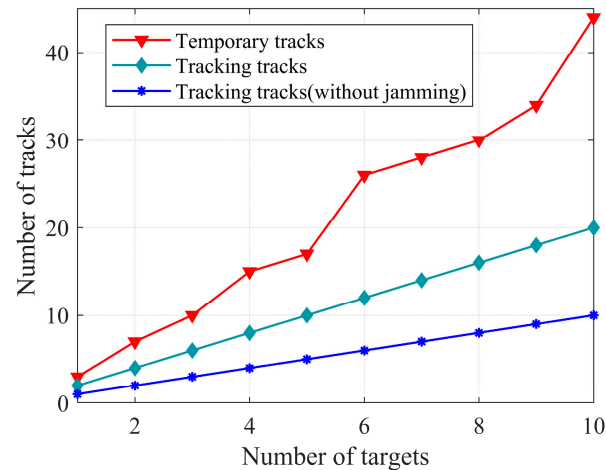


Figure 8. The influence of target number on radar track.

In Figure 8, with the interference of PSS, both tracks increased with the number of targets, with a greater increase in temporary tracks. Both tracking tracks and temporary tracks reached a number of targets that were three times greater or more; this was influenced by the false targets. In this case, some of the tracking resources were taken up and consumed. In the above simulation results, the number of temporary tracks always exceeded the tracking track. Multiple false targets caused the system to produce many redundant tracks that were unrelated to the real target, achieving the goal of disrupting radar track processing.

5. Discussion

This paper investigated the PSS modulation's effect on the radar operation tracking process. The proposed method was verified using a complete radar detection and tracking procedure. Most of the existing research on PSS is limited to its absorption performance and material design, and less attention has been paid to the effect of its modulated echo signal on radar tracks [13–16]. Using the characteristics of PSS-modulated signals for track deception is a novel research direction.

The current tracking radar countermeasures tend to use deception jamming because the active emission of a high-power noise jamming signal can be very easily traced and combated. The existing track deception jamming techniques implemented by DRFM have suffered from a low number and fidelity of false targets [5–7]. These methods require that the incident signal be intercepted, followed by the analysis and calculation of the corresponding jamming signal. Eventually, the radar jammer transmitted the signal; however, this could easily reveal the location of the jammer. For DRFM devices, their operation and calculation are more complicated and require a priori information [28]. Applying PSS to track deception can reduce the complex experimental design and achieve the same flexible modulation of the jamming effect [23–27]. The deception jamming based on PSS can respond to radar in real-time and does not actively radiate electromagnetic energy to the outside world, greatly reducing the risk of its own exposure. With the appropriate

modulation parameters, false tracks could be generated while real tracks could be faded, greatly improving the survivability of high-value targets.

In this application, the fabricated PSS could be attached to the surface of the target, and the modulation effect was more accurate because it possessed the electromagnetic scattering characteristics of the real target. However, attaching the PSS completely to the surface could affect the structural function of the protected target body and reduce its functionality; therefore, this method is not always feasible. In addition, we could make the PSS into decoys of a similar shape and size to the protected target and generate more decoys by modulating them accordingly for the purpose of deceiving the radar system.

A limitation of the current study is that the actual effect has not been demonstrated experimentally at present; we aim to focus on this in future research. In addition, the false tracks generated by this method were limited to the distance dimension, and distance-azimuth two-dimensional deception has yet to be achieved [5–7]. In existing studies, PSS has shown more severe restrictions on the angle and frequency of the incident signal in practical experiments, which is one of the reasons why PSS material design is more popular. In practice, this may be influenced by the actual environment, e.g., the undulation of the target RCS, the start of the track in the clutter environment, which may cause discrepancies, etc. Subsequent research should investigate on the impact of target electromagnetic modulation on radar data processing in different complex environments.

6. Conclusions

This paper proposes a track deception jamming method for a range of false targets based on target electromagnetic modulation. The electromagnetic modulation principle and modulation signal model of PSS have been described. Subsequently, the CFAR detection and target tracking process was analyzed, and PSS's ability to create a high-fidelity false track was demonstrated. On this basis, the number of false tracks could be flexibly changed by controlling the parameters of the PSS. In order to investigate the effect of modulation key parameters on radar tracks, different modulation frequencies and modulation duty ratios were set in the simulation. The simulation results show that the modulation frequency was inversely proportional to the number of radar tracks with a constant duty ratio. The number of tracks was symmetrically distributed with the duty ratio of 0.5 as the center, under the condition of a constant modulation frequency. The number of tracks was proportional to the duty ratio, which ranges from 0 to 0.5. The radar tracking tracks were substantially increased by PSS modulation compared to unmodulated tracks, and many redundant temporary tracks were generated, which inevitably affected the normal radar operation process. The effectiveness of the method was verified by simulating the radar tracking process under PSS jamming.

Author Contributions: Conceptualization, G.H.; Funding acquisition, J.W.; Investigation, Z.Z.; Methodology, G.H. and D.F.; Project administration, J.W.; Resources, L.W.; Software, G.H. and D.F.; Supervision, D.F. and L.W.; Validation, G.H.; Writing—original draft, G.H.; Writing—review and editing, J.W. All authors have read and agreed to the published version of the manuscript.

Funding: This research was funded by the National Natural Science Foundation of China, grant number 62201589.

Data Availability Statement: The data that support the findings of this study are available from the corresponding author upon reasonable request.

Conflicts of Interest: The authors declare no conflict of interest.

References

1. He, Y.; Xiu, J.; Zhang, J.; Guan, X. *Radar Data Processing with Applications*, 2nd ed.; Publishing House of Electronics Industry: Beijing, China, 2009; pp. 289–300.
2. Purvis, K.B.; Chandler, P.R.; Pachter, M. Feasible flight paths for cooperative generation of a phantom radar track. *J. Guid. Control. Dyn.* **2006**, *29*, 653–661. [[CrossRef](#)]

3. Zhou, C.; Liu, Q.; Chen, X. Parameter estimation and suppression for DRFM-based interrupted sampling repeater jammer. *IET Radar Sonar Navig.* **2018**, *12*, 56–63. [[CrossRef](#)]
4. Ratnoo, A.; Shima, T. Formation-flying guidance for cooperative radar deception (Article). *J. Guid. Control Dyn.* **2012**, *35*, 1730–1739. [[CrossRef](#)]
5. Iqbal, Y.; Jawad, M. An Effective Coherent Noise Jamming Method for Deception of Wideband LFM Radars. In Proceedings of the 2020 17th International Bhurban Conference on Applied Sciences and Technology (IBCAST), Islamabad, Pakistan, 14–18 January 2020.
6. Rao, B.; Gu, Z.; Nie, Y. Deception Approach to Track-to-Track Radar Fusion Using Noncoherent Dual-Source Jamming. *IEEE Access* **2020**, *8*, 50843–50858. [[CrossRef](#)]
7. Zhao, Y.; Tian, B.; Wang, C.; Gong, J.; Tan, M.; Zhou, C. Research on main-lobe deceptive jamming against FDA-MIMO radar. *IET Radar Sonar Navig.* **2021**, *15*, 641–654. [[CrossRef](#)]
8. Luo, Y.; Guo, L.; Zuo, Y.; Liu, W. Time-Domain Scattering Characteristics and Jamming Effectiveness in Corner Reflectors. *IEEE Access* **2021**, *9*, 15696–15707. [[CrossRef](#)]
9. Wang, J.; Feng, D.; Xu, Z.; Wu, Q.; Hu, W. Time-domain digital-coding active frequency selective surface absorber/reflector and its imaging characteristics. *IEEE Trans. Antennas Propag.* **2021**, *69*, 3322–3331. [[CrossRef](#)]
10. Phon, R.; Ghosh, S.; Sungjoon, L. Novel multifunctional reconfigurable active frequency selective surface. *IEEE Trans. Antennas Propag.* **2018**, *67*, 1709–1718. [[CrossRef](#)]
11. Shah, G.; Cao, Q.; Dayo, Z.A.; Azeem, M. Double Layer Multifunction Frequency Selective Surface Equipped with a Tricharacteristic Response. *IEEE Trans. Electromagn. Compat.* **2022**, *64*, 295–302. [[CrossRef](#)]
12. Zhao, Y.; Fu, J.; Wang, Z.; Chen, W.; Lv, B.; Zhang, Q. Design of a Broadband Switchable Active Frequency Selective Surfaces Based on Modified Diode Model. *IEEE Antennas Wirel. Propag. Lett.* **2022**, *21*, 1378–1382. [[CrossRef](#)]
13. Chang, Y.; Wang, L.; Li, B.; Jiao, W. Phase Switched Screen for Radar Cloaking Based on Reconfigurable Artificial Magnetic Conductor. *IEEE Trans. Electromagn. Compat.* **2021**, *63*, 1417–1422. [[CrossRef](#)]
14. Chang, Y.; Jiang, H.; Wang, L.; Ding, K. Tri-band phase switched screen based on time modulation. *Int. J. RF Microw. Comput.-Aided Eng.* **2022**, *32*, e23058. [[CrossRef](#)]
15. Ramaccia, D.; Sounas, D.L.; Alu, A.; Toscano, A.; Bilotti, F. Phase-induced frequency conversion and Doppler effect with time modulated metasurfaces. *IEEE Antennas Wirel. Propag. Mag.* **2020**, *68*, 1607–1617. [[CrossRef](#)]
16. Tennant, A.; Chambers, B. Experimental performance of a phaseswitched screen against modulated microwave signals. *IEE Proc. Radar Sonar Navigat.* **2005**, *152*, 29–33. [[CrossRef](#)]
17. Cui, T.; Liu, S.; Zhang, L. Information metamaterials and metasurfaces. *J. Mater. Chem. C* **2017**, *5*, 3644–3668. [[CrossRef](#)]
18. Cui, T.J.; Li, L.; Liu, S.; Ma, Q.; Zhang, L.; Wan, X.; Cheng, Q. Information Metamaterial Systems. *iScience* **2020**, *23*, 101403. [[CrossRef](#)]
19. Chen, M.Z.; Tang, W.; Dai, J.Y.; Ke, J.C.; Zhang, L.; Zhang, C.; Cui, T.J. Accurate and broadband manipulations of harmonic amplitudes and phases to reach 256 QAM millimeter-wave wireless communications by time-domain digital coding metasurface. *Natl. Sci. Rev.* **2022**, *9*, nwab134. [[CrossRef](#)]
20. Chambers, B.; Tennant, A. The phase-switched screen. *IEEE Antennas Propag. Mag.* **2004**, *19*, 23–27. [[CrossRef](#)]
21. Chambers, B.; Tennant, A. Influence of switching-waveform characteristics on the performance of a single-layer-phase switched screen. *IEEE Trans. Electromagn. Compat.* **2002**, *44*, 434–441. [[CrossRef](#)]
22. Xiong, Y. Electromagnetic Properties of Radar Absorbing Materials Based on Phase Modulated Surface. Master’s Thesis, Nanjing University of Aeronautics and Astronautics, Nanjing, China, 2008.
23. Feng, D.; Xu, L.; Zhang, R.; Wang, J. A study on signature of radar echo from a phase-switched screen. *Modem Radar* **2018**, *40*, 77–82.
24. Zhang, R.; Feng, D.; Xu, L. Signature of passive decoy and its application in angular deception jamming based on phase switched surface. In Proceedings of the 2016 CIE International Conference on Radar (RADAR), Guangzhou, China, 10–13 October 2016.
25. Xu, L.; Feng, D.; Zhang, R.; Wang, X. High-Resolution Range Profile Deception Method Based on Phase-Switched Screen. *IEEE Antennas Wirel.* **2016**, *15*, 1665–1668. [[CrossRef](#)]
26. Xu, L.; Feng, D.; Wang, X. Matched-filter properties of linear-frequency-modulation radar signal reflected from a phase-switched screen. *IET Radar Sonar Navig.* **2016**, *10*, 318–324. [[CrossRef](#)]
27. Fan, C.; Zhang, R.; Feng, D.; Wang, J. Resource consumption evaluation of active target control in phased array radar search. *Modem Radar* **2021**, *43*, 27–35.
28. Solomon, J.F. Defending the Fleet from China’s Antiship Ballistic Missile: Naval Deception’s Roles in Seabased Missile Defense. Master’s Thesis, Georgetown University, Washington, DC, USA, 2011.

Disclaimer/Publisher’s Note: The statements, opinions and data contained in all publications are solely those of the individual author(s) and contributor(s) and not of MDPI and/or the editor(s). MDPI and/or the editor(s) disclaim responsibility for any injury to people or property resulting from any ideas, methods, instructions or products referred to in the content.